Mid-band PPN InGaN solar cell for indoor visible light communication in 5G/6G applications

Habib Ullah Manzoor (habibullahmanzoor@gmail.com)
University of Glasgow https://orcid.org/0000-0003-0192-7353
Ng Sha Shiong
Universiti Sains Malaysia
Arooj Aslam
Riphah International University
Tareq Manzoor
COMSATS University Islamabad - Lahore Campus

Research Article

Keywords: III–V nitride, Semiconducting indium compounds, Solar energy, Photovoltaics, Optical communication, SCAPS-1D

Posted Date: March 2nd, 2022

DOI: https://doi.org/10.21203/rs.3.rs-1384501/v1

Abstract

Recently, solar cells have been simultaneously used as energy harvester and receiver in free-space optical (FSO) communication networks. In this study, a mid-band p-$In_{0.01}Ga_{0.99}N$/p-$In_{0.5}Ga_{0.5}N$/n-$In_{0.5}Ga_{0.5}N$ (PPN) solar cell that achieved a conversion efficiency of 26.36% (under 1.5 AM condition) was used as a receiver for an indoor FSO communication network. Considering that this solar cell had a length and width of 1 mm, the FSO system was simulated using Optisystm software. Meanwhile, the solar cell was simulated using SCAPS-1D software. The power received from the solar cell was compared with those of four commercially available avalanche photodiode (APD) receivers. Incident wavelength was varied in the visible region from 400 nm to 700 nm for transmission lengths of 5, 10, 15, and 20 m. The current–voltage and power–voltage curves were presented at different incident wavelengths and transmission distances. The InGaN solar cell provides more electrical power than all the commercial APDs. In conclusion, an increase in received power can improve the quality of an FSO network and support longer transmission length.

Introduction

5G is expected to increase the capacity of modern communication networks by up to 1000-fold [1],[2]. The growth of a network's capacity in radio-frequency communication has been established as restricted due to limited spectrum resources [3],[4]. In the near future, the downlink data rate can reach 20 Gb/s while uplink can reach 10 Gb/s [5]. To compensate for the growing demands, many scientists are considering the use of light as a communication medium [6]-[7].

Free-space optical (FSO) communication uses light as a communication channel in wireless environments. It is also known as optical wireless communication (OWC). Recent advancements in communication networks require huge bandwidth and prime quality networks. Radio-frequency networks provide limited speed, whereas FSO communication networks provide wide bandwidth without frequency regulations [8],[9]. Moreover, FSO communication exhibits many advantages over traditional communication systems. These advantages include high bandwidth (up to 2000 THz), narrow beamwidth, unlicensed spectrum, low installation cost, and easy development and redevelopment [10]. In the past, FSO systems were used in military applications [11] and inter-satellite links [12]. Recently, some companies have offered newly developed equipment for FSO communication systems [13]-[14]. Such initiative promises a new growing market of communication systems.

In general, OWC systems have five types, depending upon the transmission distance:

(i)Ultrashort range, e.g., chip-to-chip communication [15];

(ii) Short range, e.g., wireless body area network [16]; wireless personal area network, and underwater communication [17];
(iii) Medium range, e.g., indoor infrared and visible light communication (VLC) for wireless local area networks [18];

(iv) Long range, e.g., inter-building connections; and
(v) Ultralong range, e.g., inter-satellite [19] and deep space [20] links.
An OWC network that can provide 100 Gbps was achieved at indoor illuminations [21]. Moreover, optical communication networks supports the emerging trend toward energy-efficient communication networks [22],[23]. OWC technology does not require extensive hardware; hence, a low cost and green agenda can be achieved.[24] Light cannot pass through walls, and thus, OWC can also provide high security [25].

In modern light communication systems, either a laser or light-emitting diode (LED) is used to transmit light,[9] and a PIN diode or avalanche photodiode (APD) is used as a receiver [26]. In 2013, Kim and Won proposed that solar cells can be used simultaneously as a receiver in an FSO communication system and as a renewable energy source for producing electricity.[27] They used LED and a silicon solar cell to archive ~ 10 kHz bandwidth through a transmission distance of 40 cm. Consequently, their study became the basis for using solar cells as optical receivers. In 2015, Wang et al. designed an OWC system that utilizes a polycrystalline silicon solar cell to receive light and harvest energy [28]. In 2018, a single junction GaAs solar cell with a diameter of 1 mm was used for an FSO communication system [29]. In addition, the use of an organic solar cell (PTB7:PC71BM)[30] and a triple junction perovskite solar cell[31] were reported for receiving light and harvesting solar energy. Despite the large number of reported studies, the use of InGaN solar cells in FSO communication systems has yet to be explored.

Recently, third-generation solar cells, including InGaN solar cells, have been actively investigated for obtaining high conversion efficiency [32]-[33]. InGaN alloy has exhibited potential in photodetectors, electronic devices,[34] and laser diodes [35]. One of the unique properties of an InGaN material is its tunable direct wide bandgap ranging from 0.7 eV (InN) to 3.4 2 eV (GaN) [36]. Considering its excellent thermal stability and high mobility, an InGaN material can replace silicon in many high-frequency optoelectronic and electronic applications in harsh environments [37],[38].

The current study explores the use of an InGaN-based solar cell as a receiver in an FSO communication network for indoor applications. A single-channel 100 Gbps FSO network was evaluated. The results of an FSO communication system with a mid-band p-$In_{0.01}Ga_{0.99}N$/p-$In_{0.5}Ga_{0.5}N$/n-$In_{0.5}Ga_{0.5}N$ (PPN) solar cell as an optical receiver was compared with that of an FSO system with a traditional optical receiver. The FSO communication system was created using Optisystem software, and the solar cell was evaluated using SCAPS-1D software. The considered incident light was varied from 400 nm to 700 nm, and the FSO communication systems were evaluated on the basis of the received electrical power.

Experimental Setup

2.1 THEROTICAL SIMULATION

A 100 Gbps single channel that used on–off keying (OOK) modulation was created using Optisystem software. Optisytem was developed by Optiwave System Inc., and it can be used to simulate all types of optical communication systems. The considered OOK FSO network has three major parts: the transmitter,

the FSO channel, and the receiver. The downlink transmitter consists of a not return-to-zero pulse generator with a duty cycle of 0.5 bit, driven by a pseudo-random bit sequence generator to generate a data rate of 100 Gbps, modulated by a continuous wavelength (CW) laser by using a Mach–Zehnder modulator. The CW laser was operated at a power of − 20 dBm, and it had a wavelength, λ, ranging from 400 nm to 700 nm. The light produced from the Mach–Zehnder modulator was passed through the FSO channel with four different transmission lengths (5, 10, 15, and 20 m). The FSO channels had an attenuation of 25 dB/km and a beam divergence of 2 mrad. An avalanche photodiode (APD) with a responsivity of 1 A/W, a dark current of 10 nA, and a low-pass filter with a cutoff frequency of 0.75 × bit rate was used as the receiver to convert optical signals into electrical signals, as shown in Fig. 1. An eye diagram visualizer was used to obtain eye diagrams of all the FSO channels at the receiving end to ensure that the FSO communication was working correctly, as shown in Fig. 2.

2.2 Free-space network

Figures 2(a), 2(b), 2(c), and 2(d) represent the eye diagrams at 20, 15, 10, and 5 m, respectively, when λ = 700 nm. The eye diagrams are clearer at a transmission distance of 5 m than at a transmission distance of 20 m because a longer transmission distance results in more attenuation losses. The height of the received eye diagram at transmission distances of 20, 15, 10, and 5 m is 1.01×10^{-4}, 1.37×10^{-4}, 1.95×10^{-4}, and 2.91×10^{-4} a.u., respectively. An optical power meter was used at the end of the FSO channel to obtain the received optical power, while an electrical power meter was used at the receiver to measure the received electrical power. Different commercially available APDs that can be used in the visible light region are listed in Table 1. They are APD15-8-150-T5H, APD230-LCC, MTAPD-06-001, and APD120A2. These APDs are manufactured by OSI Optoelectronics, Roithner Laser Technik, Marktech Optoelectronics, and Thorlabs, respectively. The results of the received optical and electrical powers are summarized in Table 2. The table indicates that the APDs perform better toward the longer side of the wavelength because the output of the optical receivers, including APD, depends upon responsivity [39]. The photocurrent in APD is proportional to the applied power when the proportionality constant is responsivity [40]. Responsivity, R, can be defined as [39]

$$\mathrm{R} \approx \frac{\eta\lambda}{1.24} \tag{1}$$

From Eq. (1), R evidently increases with an increase in the applied wavelength of light.

Table 1
Parameters of commercially available APDs.

ADP	Company name	Diameter (mm)	Wavelength (nm)	Dark current (nA)	Responsivity at (400–700 nm) (A/W)
APD15-8-150-T5H	OSI Optoelectronics	1.5	800	0.50	2–40
APD230-LCC	Roithner Laser Technik	230.00	400–1100	0.20	0.5–27
MTAPD-06-001	Marktech Optoelectronics	0.230	400–1100	0.05	5–40
APD120A2	Thorlabs	1	200–1000	-	12–25

2.3 InGaN-based solar cell

In this work, the InGaN-based solar cell consists of a three-layered PPN InGaN structure [41]. The top layer is p-In0.01GaN0.99 with a thickness of 0.1 μm, while the middle and bottom layers are made of 1.0 μm-thick p-In0.5GaN0.5 and n-In0.01GaN0.99 layers, respectively, as shown in Fig. 3. All the layers have a carrier density of 1019 cm^{-3}. All the parameters of the InGaN material used in the simulation are listed in Table 3. The performance of this solar cell was simulated using SCAPS-1D software with a solar spectrum of 1.5 AM at a temperature of 300 K.

Figure 4 shows the current–voltage (I–V) and power–voltage (P–V) curves of the PPN solar cell. The simulation results indicates that the cell can provide an open circuit voltage, Voc, of 1.32 V; a current density, Jsc, of 21.95 mA/cm^2; a fill factor of 90.37%; and a conversion efficiency, η, of 26.36%. This cell can provide a power density of 26.4 mW/cm^2.

Table 2
Received optical and electrical powers when ADP is used as the receiver.

Wavelength, λ (nm)	Transmission distance (m)	Received optical power (W)	Received electrical power (W)			
			APD15-8-150-T5H	APD230-LCC	MTAPD-06-001	APD120A2
700	20	2.13E-05	1.35E-06	6.16E-07	1.35E-06	3.90E-07
	15	2.78E-05	2.25E-06	9.40E-06	2.29E-06	6.62E-07
	10	3.73E-05	4.13E-06	1.70E-05	4.14E-06	1.19E-06
	5	5.23E-05	8.13E-06	3.33E-05	8.13E-06	2.34E-06
600	20	2.13E-05	3.38E-07	3.38E-07	6.16E-07	5.07E-07
	15	2.78E-05	5.73E-07	5.15E-06	1.04E-06	8.60E-07
	10	3.73E-05	1.03E-06	9.32E-06	1.88E-06	1.55E-06
	5	5.23E-05	2.03E-06	1.83E-05	3.70E-06	3.05E-06
500	20	2.13E-05	2.11E-08	1.66E-07	6.84E-08	3.38E-07
	15	2.78E-05	3.58E-08	2.52E-06	1.16E-07	5.73E-07
	10	3.73E-05	6.48E-08	4.56E-06	2.10E-07	1.04E-06
	5	5.23E-05	1.27E-07	8.96E-06	4.12E-07	2.02E-06
400	20	2.13E-05	3.39E-09	2.28E-10	1.35E-08	1.22E-07
	15	2.78E-05	5.75E-09	3.25E-09	2.29E-08	2.06E-07
	10	3.73E-05	1.04E-08	5.85E-09	4.15E-08	3.73E-07
	5	5.23E-05	2.03E-08	1.15E-08	8.13E-08	3.72E-07

Table 3
Parameters of the InGaN solar cell.

No.	Parameter	Value/Related equation
1	Bandgap, Eg [36]	$x.E_g^{InN} + (1-x).E_g^{GaN} - b.x.(1-x)$ Here, x = 0 – 1, E_g^{InN} is 0.7 eV, and E_g^{GaN} is 3.42 eV. b is known as the bowing factor, which is equal to 1.43 eV.
2	Electron affinity, χ [48]	$4.1 + 0.7(3.4 - E_g)$
3	Relative permittivity, ε [49]	$15.3x + 8.9(1-x)$
4	Effective density state of the conduction band Nc [50]	$(0.9x + 2.3(1-x)) \times 10^{18}\ cm^{-3}$
5	Effective density state of the valance band Nv [50]:	$(5.3x + 1.8(1-x)) \times 10^{19}\ cm^{-3}$
6	Carrier concentration	$1\times10^{19}\ cm^{-3}$
7	Capture cross-section electrons	$1.0\times10^{-15}\ cm^{2}$
8	Capture cross-section holes	$1.0\times10^{-15}\ cm^{2}$
9	Defect density	$1.0\times10^{14}\ cm^{-3}$

2.4 SOLAR CELL AS RECIEVER

Figure 5 shows the schematic of a single-channel OOK FSO communication system with the PPN solar cell as receiver. The dimensions of the cell are 1 mm × 1 mm.

A series of simulations was conducted using SCAPS-1D software. The power of the incident light was adjusted as the received optical power from Optisystem software, as mentioned in Table 2. The simulations were performed at different incident wavelengths of the visible spectrum, i.e., λ = 400 nm to 700 nm. The obtained results were summarized in Table 4 and plotted in Fig. 6. The highest power was produced when λ = 700 nm, and it was used due to an increase in responsivity at λ = 700 nm. As λ decreased, the received electrical power was reduced. However, better results were still obtained than those of all commercially available APDs.

Results And Discussion

A comparison of Tables 2 and 4 implies that the solar cell provides better results than the APD receiver for FSO communication networks due to the former's better spectral response. The responsivity of the PPN solar cell can be measured using Eq. (2)[42]:

$$\text{SpectralResponse} = \frac{\text{QuantumEfficiency} \times \text{IncidentWavelength(nm)}}{1239.8}$$

2

The quantum efficiency of the PPN solar cell is presented in Fig. 7. The responsivity of the PPN solar cell varied from 54 A/W to 34 A/W when the incident wavelength was reduced from 700 nm to 400 nm. A comparison with Table 1 implies that the PPN solar cell provides better spectral response than APD15-8-150-T5H, APD230-LCC, MTAPD-06-001, and APD120A2; and thus, it produces more output power. The spectral responses of APD15-8-150-T5H, APD230-LCC, MTAPD-06-001, and APD120A2 were obtained from their datasheets and listed in Table 1.

Table 4
Received optical and electrical powers of a single-channel OOK FSO communication system with the PPN solar cell as receiver

Wavelength, λ (nm)	Transmission distance (m)	Received optical power (W)	Received electrical power (W)
700	20	2.13E-05	1.28E-05
	15	2.78E-05	1.66E-05
	10	3.73E-05	2.25E-05
	5	5.23E-05	3.20E-05
600	20	2.13E-05	1.15E-05
	15	2.78E-05	1.50E-05
	10	3.73E-05	2.02E-05
	5	5.23E-05	2.87E-05
500	20	2.13E-05	9.65E-06
	15	2.78E-05	1.25E-05
	10	3.73E-05	1.69E-05
	5	5.23E-05	2.39E-05
400y	20	2.13E-05	8.67E-06
	15	2.78E-05	1.12E-05
	10	3.73E-05	1.52E-05
	5	5.23E-05	2.15E-05

The I–V and P–V curves at different incident wavelengths and transmission lengths are presented in Figs. 8(a)–8(d). The performance of the InGaN solar cell decreased when the incident wavelength was reduced from 700 nm to 400 nm. This behavior can be explained by the responsivity of the PPN solar cell.

An average optical power of 3.47E-05 W produces an average electrical power of 1.26E-06, 8.33E-07, 1.51E-06, and 9.75E-07 W by using APD15-8-150-T5H, APD230-LCC, MTAPD-06-001, and APD120A2, respectively. Meanwhile, the InGaN solar cell produces 1.74E-05 W. The cell, PPN produces 13.9, 20.9, 16.1, and 17.9 times more power than APD15-8-150-T5H, APD230-LCC, MTAPD-06-001, and APD120A2, respectively. All the commercially available APDs used in this work are made of silicon. The PPN solar cell can be implied to perform better as receiver in VLC due to its better spectral response.

The use of solar cells with low energy-consuming devices can lead to self-powered networks [43]. Self-power can further reduce the overall system cost by eliminating the costs of battery and human interaction [44]. In self-powered networks, energy from solar cells can be used to run devices, such as body-mounted sensors,[45] pollution monitoring devices,[46] and medical devices [54].

Conclusion

In the current study, a three-layered PPN solar cell with 26.36% conversion efficiency under 1.5 AM condition was used as an optical receiver for indoor FSO applications that used visible light. Simulations were conducted for a 100 Gbps downlink channel by using the OOK modulation format in an FSO communication network with four commercially available APDs and a PPN (InGaN-based) solar cell as the receiver. The PPN solar cell can provide more output power than the commercially available APDs (APD15-8-150-T5H, APD230-LCC, MTAPD-06-001, and APD120A2). The increased output power will contribute to the improved performance of the received signal, i.e., the bit error rate, Q factor, and height of the eye diagram. The increased output power can also support a longer transmission distance.

Future Work

The PPN solar cell can provide more output power than APDs. However, its effects on the improvement of the supported data rate, bit error rate, and Q factor must be studied further.

Declarations

Acknowledgment

The authors would like to thank Mr. Marc Burgelman for his assistance in the development of the SCAPS-1D software.

Competing interests

The authors have no relevant financial or non-financial interests to disclose.

Funding

No funding was acquired for this study

Statements & Declarations

The authors declare that no funds, grants, or other support were received during the preparation of this manuscript.

Data availability

All simulations and generated data can be provided by requesting corresponding author.

Author contribution

Habib Ullah Manzoor: Conceptualization, Methodology, Software, Writing - Original Draft, Resources, Validation.

Ng Sha Shiong: Validation, Formal analysis, Writing - Review & Editing, Supervision.

Arooj Aslam: Validation, Writing - Review & Editing.

Tareq Manzoor: Project administration, Validation.

References

1. Boccardi, F., Heath, R., Lozano, A., Marzetta, T.L., Popovski, P.: Five disruptive technology directions for 5G. IEEE Commun. Mag. **52**(2), 74–80 (2014). doi:10.1109/MCOM.2014.6736746. “,”, ,
2. Larsson, E.G., Edfors, O., Tufvesson, F., Marzetta, T.L.: Massive MIMO for next generation wireless systems. IEEE Commun. Mag. **52**(2), 186–195 (2014). doi:10.1109/MCOM.2014.6736761. “,”, ,
3. Salhab, A.M., Alouini, M.-S., Obeed, M., Zummo, S.A., “Joint Optimization of Power Allocation and Load Balancing for Hybrid VLC/RF Networks,” *J. Opt. Commun. Networking, Vol. 10, Issue 5, pp. 553–562*, vol. 10, no. 5, pp. 553–562, May: 2018, doi: 10.1364/JOCN.10.000553
4. Ghassemlooy, Z., Arnon, S., Uysal, M., Xu, Z., Cheng, J., “Emerging Optical Wireless Communications-Advances and Challenges,” *IEEE J. Sel. Areas Commun.*, vol. 33, no. 9, pp. 1738–1749, Sep. 2015, doi: 10.1109/JSAC.2015.2458511
5. Willner, A.E., “Optical fiber telecommunications VII,” *Opt. Fiber Telecommun. VII*, pp. 1–1083, Jan. 2019, doi: 10.1016/C2017-0-03572-3
6. Koonen, T.: Indoor Optical Wireless Systems: Technology, Trends, and Applications. J. Light Technol. **36**(8), 1459–1467 (Apr. 2018). doi:10.1109/JLT.2017.2787614. “,”, ,
7. Chen, H., Van Den Boom, H.P.A., Tangdiongga, E., Koonen, T.: 30-Gb/s bidirectional transparent optical transmission with an MMF access and an indoor optical wireless link. IEEE Photonics Technol. Lett. **24**(7), 572–574 (2012). doi:10.1109/LPT.2012.2183121. “,”, ,
8. Zhang, J., Li, R., Gao, Z., Dang, A., “Ergodicity of Phase Fluctuations for Free-Space Optical Link in Atmospheric Turbulence,” *IEEE Photonics Technol. Lett.*, vol. 31, no. 5, pp. 377–380, Mar. 2019, doi: 10.1109/LPT.2019.2895886

9. M. A. K. and Uysal, M.: Survey on Free Space Optical Communication: A Communication Theory Perspective. IEEE Commun. Surv. Tutorials. **16**(4), 2231–2258 (2014). doi:10.1109/COMST.2014.2329501. “,”, ,
10. X. Z. and Kahn, J.M., “Free-space optical communication through atmospheric turbulence channels,” *EEE Trans. Commun.*, vol. 50, no. 8, pp. 1293–1300, 2002, doi: 10.1109/TCOMM.2002.800829
11. Rabinovich, W.S., et al.: Free space optical communications research at the U.S. Naval Research Laboratory. Free. Laser Commun. Technol. XXII. **7587**, 758702 (Feb. 2010). doi:10.1117/12.843682. “,”,
12. Tolker-Nielsen, T., Oppenhauser, G., “In-orbit test result of an operational optical intersatellite link between ARTEMIS and SPOT4, SILEX,” *Free. Laser Commun. Technol. XIV*, vol. 4635, pp. 1–15, Apr. 2002, doi: 10.1117/12.464105
13. Killinger, D.: Free Space Optics for Laser Communication Through the Air. Opt. Photonics News. **13**(10), 36–42 (2002). doi:https://doi.org/10.1364/OPN.13.10.000036. “,”, ,
14. Le Minh, H., et al.: A 1.25-Gb/s indoor cellular optical wireless communications demonstrator. IEEE Photonics Technol. Lett. **22**, 21, pp. 1598–1600 (2010). doi:10.1109/LPT.2010.2073696. “,”, no.
15. Feldman, M.R., Esener, S.C., Guest, C.C., Lee, S.H.: “Comparison Between Optical and Electrical Interconnections Based on Power and Speed Considerations.,” vol. 27, no. 9, pp. 105–108, 1987, doi: 10.1364/ao.27.001742
16. “802–2014 IEEE Standard for Local and Metropolitan Area Networks: Overview and Architecture.,” *IEEE Std 802–2014 (Revision to IEEE Std 802–2001)*, pp. 1–74, 2014, doi: 10.1109/IEEESTD.2014.6847097
17. Hanson, F., Radic, S., “High bandwidth underwater optical communication,” *Appl. Opt. Vol. 47, Issue 2, pp. 277–283*, vol. 47, no. 2, pp. 277–283, Jan. 2008, doi: 10.1364/AO.47.000277
18. Gfeller, F., Bapst, U.: Wireless in-house data communication via diffuse infrared radiation. Inf. Syst. **5**(3), 248 (1980). doi:10.1016/0306-4379(80)90043-5. “,”, ,
19. Chan, V.W.S., “Optical Satellite Networks,” *J. Light. Technol.*, vol. 21, no. 11, pp. 2811–2827, Nov. 2003, doi: 10.1109/JLT.2003.819534
20. Biswas, A., Srinivasan, M., Piazzolla, S., Hoppe, D.: Deep space optical communications, vol. 10524, p. 105240. U (Feb. 2018). doi:10.1117/12.2296426. “,”,
21. Tsonev, D., Haas, H., Videv, S., “Towards a 100 Gb/s visible light wireless access network,” *Opt. Express, Vol. 23, Issue 2, pp. 1627–1637*, vol. 23, no. 2, pp. 1627–1637, Jan. 2015, doi: 10.1364/OE.23.001627
22. Yang, Y., Zeng, Z., Cheng, J., Guo, C.: “A novel hybrid dimming control scheme for visible light communications,” IEEE Photonics J., 9, 6, Dec. 2017, doi:10.1109/JPHOT.2017.2771223
23. Haas, H., Yin, L., Wang, Y., Chen, C.: What is LiFi? J. Light Technol. **34**(6), 1533–1544 (Mar. 2016). doi:10.1109/JLT.2015.2510021. “,”, ,

24. Karunatilaka, D., Zafar, F., Kalavally, V., Parthiban, R., “LED based indoor visible light communications: State of the art,” *IEEE Commun. Surv. Tutorials*, vol. 17, no. 3, pp. 1649–1678, Jul. 2015, doi: 10.1109/COMST.2015.2417576
25. Zhang, Y.Y., Yu, H.Y., Zhang, J.K., Zhu, Y.J., Wang, J.L., Wang, T.: Space Codes for MIMO Optical Wireless Communications: Error Performance Criterion and Code Construction. IEEE Trans. Wirel. Commun. **16**(5), 3072–3085 (May 2017). doi:10.1109/TWC.2017.2675398. “,”, ,
26. Kong, M., et al.: Survey of energy-autonomous solar cell receivers for satellite–air–ground–ocean optical wireless communication. Prog. Quantum Electron. **74**, no. October, p. 100300 (2020). doi:10.1016/j.pquantelec.2020.100300. “,”,
27. Kim, S.-M., Won, J.-S., “Simultaneous reception of visible light communication and optical energy using a solar cell receiver,” in: 2013 *International Conference on ICT Convergence*, 2013, pp. 896–897, doi: 10.1109/ICTC.2013.6675511
28. Wang, Z., Tsonev, D., Videv, S., Haas, H., “On the Design of a Solar-Panel Receiver for Optical Wireless Communications with Simultaneous Energy Harvesting,” *IEEE J. Sel. Areas Commun.*, vol. 33, no. 8, pp. 1612–1623, Aug. 2015, doi: 10.1109/JSAC.2015.2391811
29. Fakidis, J., Videv, S., Helmers, H., Haas, H.: 0.5-Gb/s OFDM-Based Laser Data and Power Transfer Using a GaAs Photovoltaic Cell. IEEE Photonics Technol. Lett. **30**(9), 841–844 (May 2018). doi:10.1109/LPT.2018.2815273. “,”, ,
30. Tsonev, D., et al., “Organic solar cells as high-speed data detectors for visible light communication,” *Opt. Vol. 2, Issue 7, pp. 607–610*, vol. 2, no. 7, pp. 607–610, Jul. 2015, doi: 10.1364/OPTICA.2.000607
31. Turnbull, G.A., et al., “Triple-cation perovskite solar cells for visible light communications,” *Photonics Res. Vol. 8, Issue 8, pp. A16-A24*, vol. 8, no. 8, pp. A16–A24, Aug. 2020, doi: 10.1364/PRJ.393647
32. Khettou, A., et al.: Simulation and optimization of InGaN Schottky solar cells to enhance the interface quality. Superlattices Microstruct. **142**, no. April, p. 106539 (2020). doi:10.1016/j.spmi.2020.106539. “,”,
33. Jiang, C., et al., “Enhanced photocurrent in InGaN/GaN MQWs solar cells by coupling plasmonic with piezo-phototronic effect,” *Nano Energy*, vol. 57, no. December 2018, pp. 300–306, 2019, doi: 10.1016/j.nanoen.2018.12.036
34. Wierer, J.J., David, A., Megens, M.M.: III-nitride photonic-crystal light-emitting diodes with high extraction efficiency. Nat. Photonics 2009. **33, vol. 3**(3), 163–169 (Feb. 2009). doi:10.1038/nphoton.2009.21. “,”,
35. Jiang, L., et al.: GaN-based green laser diodes. J. Semicond. **37**(11), 1–10 (2016). doi:10.1088/1674-4926/37/11/111001. “,”, ,
36. Wu, J., Walukiewicz, W.: Band gaps of InN and group III nitride alloys. Superlattices Microstruct. **34**, no. 1–2 (2003). doi:10.1016/j.spmi.2004.03.069. “,”, , pp. 63–75
37. van Wyk, J.D., Lee, F.C.: On a Future for Power Electronics. IEEE J. Emerg. Sel. Top. Power Electron. **1**(2), 59–72 (2013). doi:10.1109/JESTPE.2013.2271499. “,”, ,

38. Ambacher, O.: Growth and applications of Group III-nitrides. J. Phys. D Appl. Phys. **31**(20), 2653 (1998). doi:https://doi.org/10.1088/0022-3727/31/20/001. “,”, ,
39. Agrawal, G.P.: Fiber-Optic Communication Systems, 4th edn. Wiley (2012)
40. Jacobs, I., “Optical Fiber Communication Technology and System Overview,” *Conf. Proc. - IEEE SOUTHEASTCON*, pp. 567–591, 1995, doi: 10.1007/978-94-011-0035-9_29
41. Manzoor, H.U., Zawawi, M.A.M., Pakhuruddin, M.Z., Ng, S.S., Hassan, Z.: High conversion and quantum efficiency indium-rich p-InGaN/p-InGaN/n-InGaN solar cell. Phys. B Condens. Matter. **622**, no. August, p. 413339 (2021). doi:10.1016/j.physb.2021.413339. “,”,
42. “Spectral Response | PVEducation.” https://www.pveducation.org/pvcdrom/solar-cell-operation/spectral-response (accessed Aug. 29, 2021)
43. Dondi, D., Bertacchini, A., Brunelli, D., Larcher, L., Benini, L., “Modeling and optimization of a solar energy harvester system for self-powered wireless sensor networks,” *IEEE Trans. Ind. Electron.*, vol. 55, no. 7, pp. 2759–2766, Jul. 2008, doi: 10.1109/TIE.2008.924449
44. Bi, S., Zeng, Y., Zhang, R., “Wireless powered communication networks: An overview,” *IEEE Wirel. Commun.*, vol. 23, no. 2, pp. 10–18, Apr. 2016, doi: 10.1109/MWC.2016.7462480
45. Wu, F., Redoute, J.M., Yuce, M.R., “WE-safe: A self-powered wearable IoT sensor network for safety applications based on lora,” *IEEE Access*, vol. 6, pp. 40846–40853, Jul. 2018, doi: 10.1109/ACCESS.2018.2859383
46. Wu, F., Rüdiger, C., Yuce, M.R.: “Real-Time Performance of a Self-Powered Environmental IoT Sensor Network System,” Sens. 2017, 17, Page 282, vol. 17, 2, 282, Feb. 2017, doi:10.3390/S17020282
47. Hande, A., Polk, T., Walker, W., Bhatia, D., “Self-Powered Wireless Sensor Networks for Remote Patient Monitoring in Hospitals,” *Sensors 2006, Vol. 6, Pages 1102–1117*, vol. 6, no. 9, pp. 1102–1117, Sep. 2006, doi: 10.3390/S6091102
48. Nawaz, M., Ahmad, A.: “A TCAD-based modeling of GaN/InGaN/Si solar cells,” Semicond. Sci. Technol., 27, 3, 2012, doi:10.1088/0268-1242/27/3/035019
49. Zhang, X., et al., “Simulation of In0.65Ga0.35 N single-junction solar cell,” *J. Phys. D. Appl. Phys.*, vol. 40, no. 23, pp. 7335–7338, 2007, doi: 10.1088/0022-3727/40/23/013
50. Goldberg, Y., Levinshtein, M., Rumyantsev, S.: “Advanced semiconductor materials,” pp. 93–143, 2001

Figures

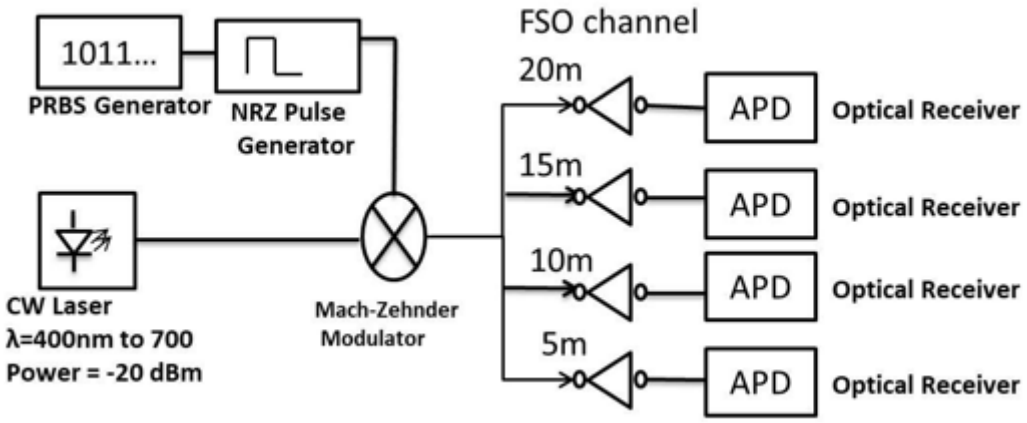

Figure 1

Schematic of the single-channel OOK FSO communication system.

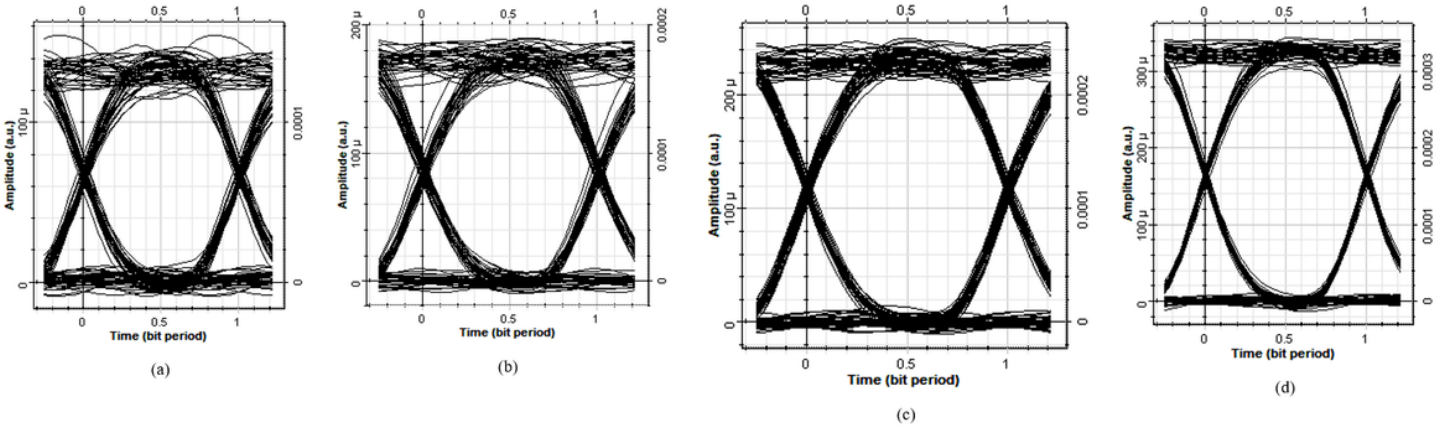

Figure 2

Eye diagram at the receiving end for transmission distances of (a) 20 m, (b) 15 m, (c) 10 m, and (d) 5 m at an incident wavelength λ =700 nm.

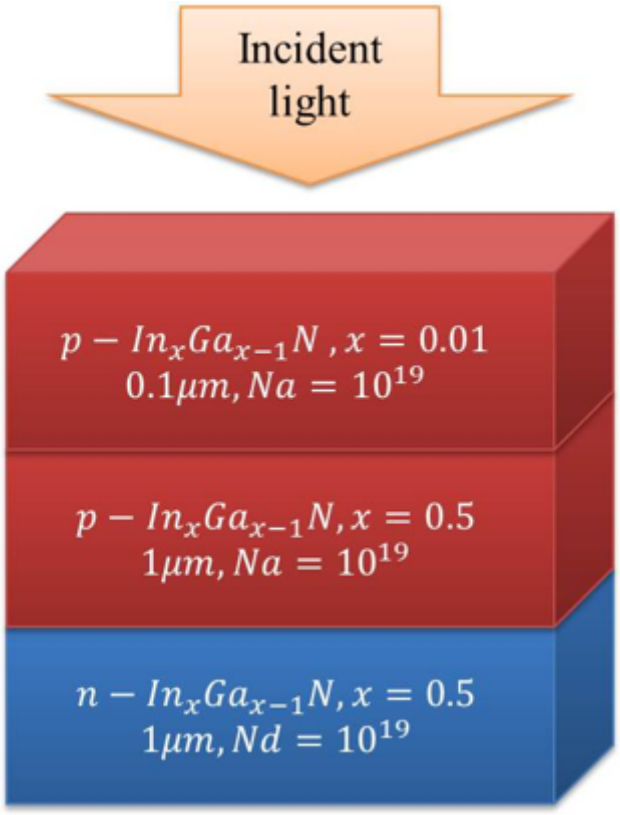

Figure 3

PPN solar cell.

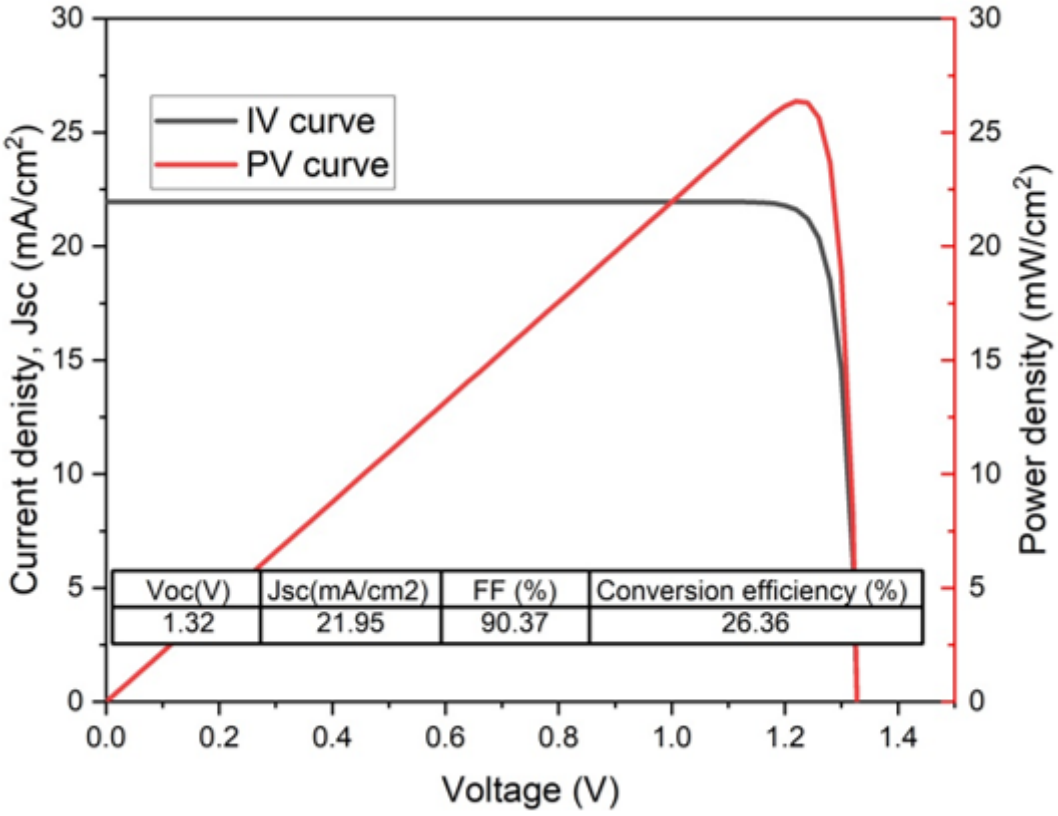

Figure 4

I–V and P–V curves of the PPN InGaN-based solar cell under 1.5 AM condition at a temperature of 300 K.

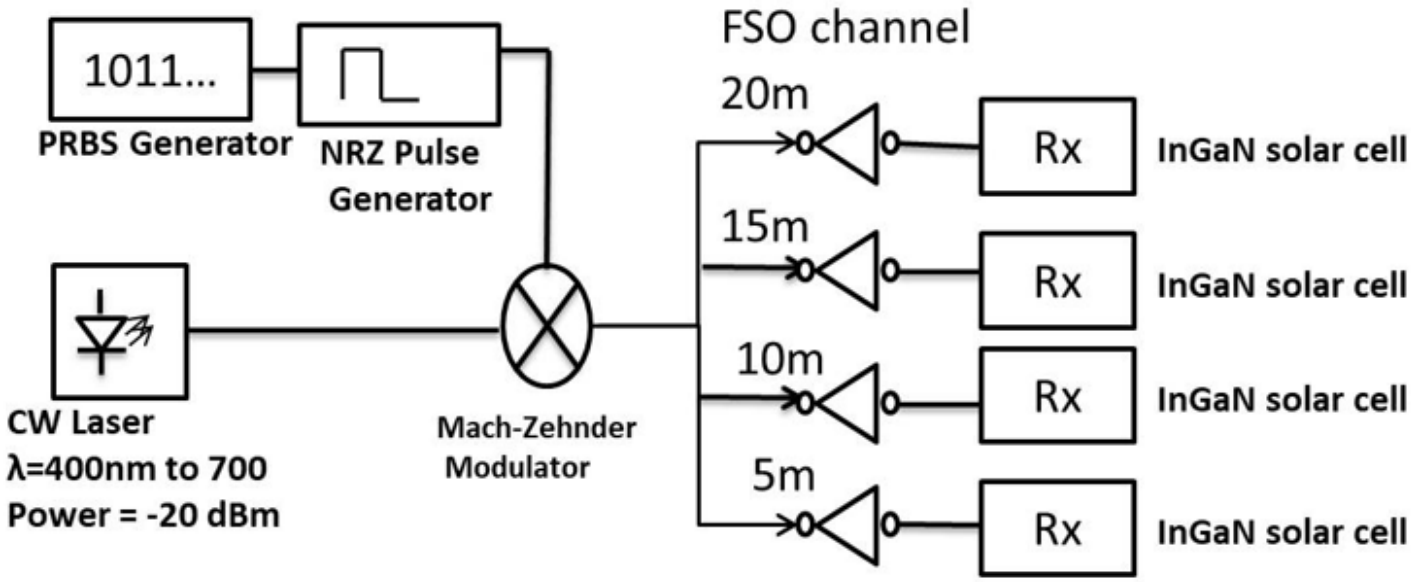

Figure 5

Schematic of a single-channel OOK FSO communication system with a PPN solar cell as receiver.

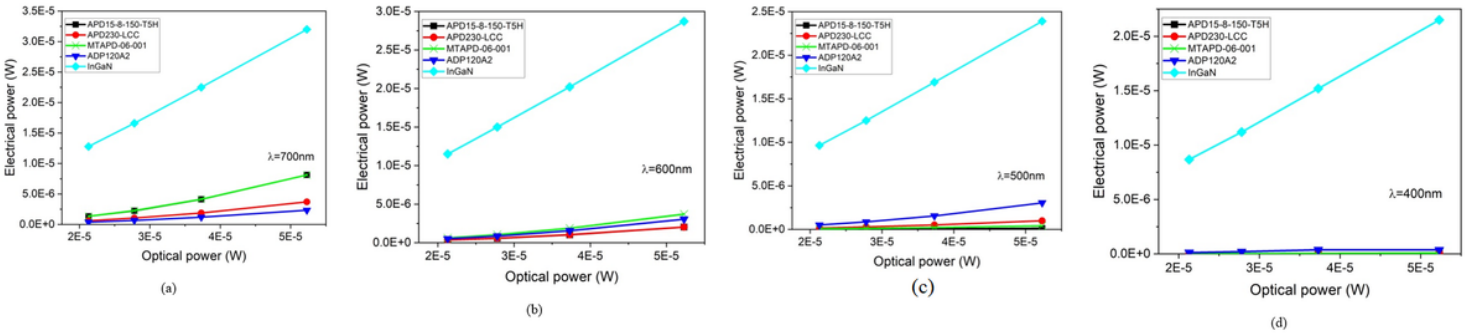

Figure 6

Received electrical power at the end of the FSO channel at different incident wavelengths (a) 700nm (b) 600nm (c) 500nm (d) 400nm.

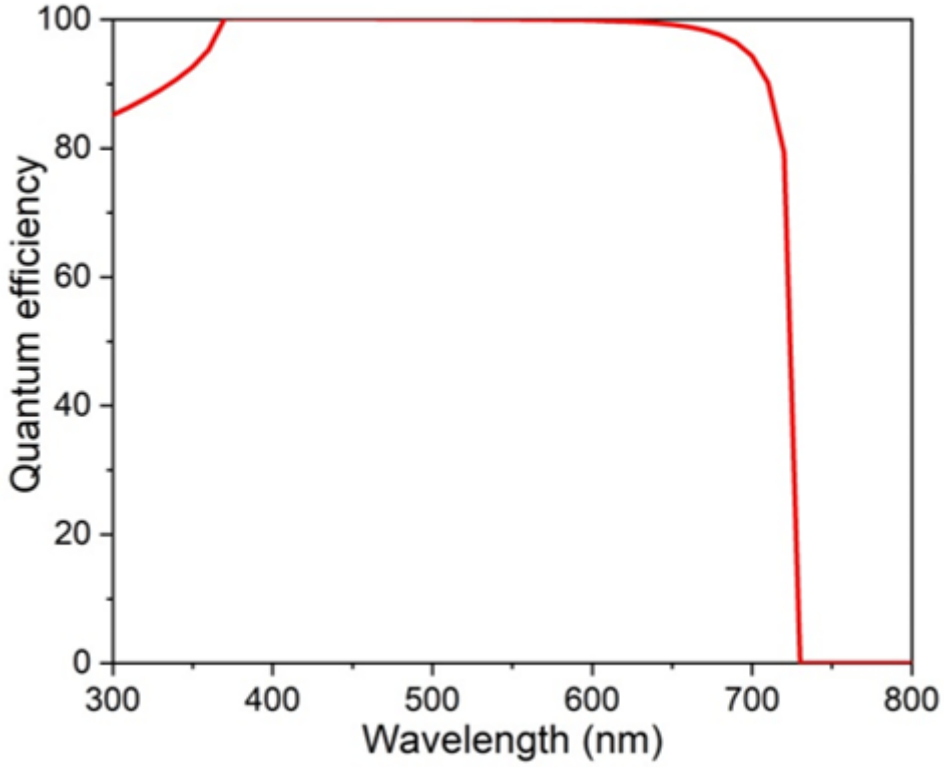

Figure 7

Quantum efficiency of the PPN solar cell.

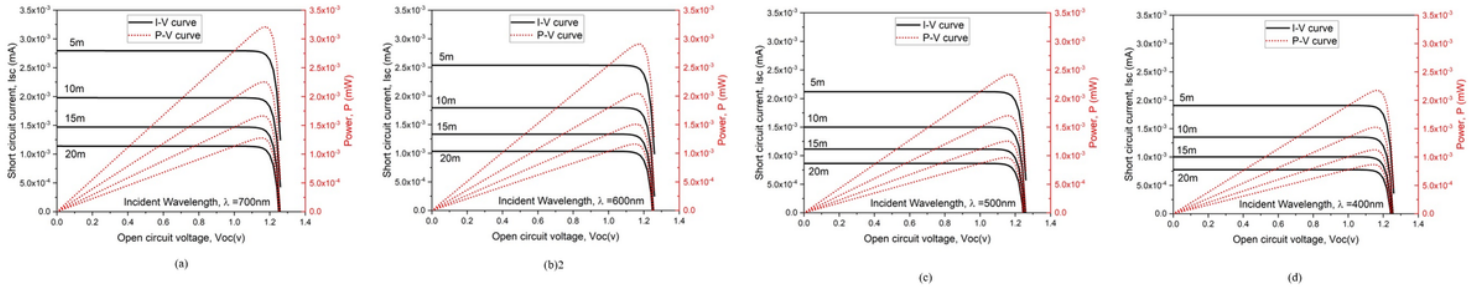

Figure 8

I–V and P–V curves at different transmission lengths and incident wavelengths: λ = (a) 700 nm, (b) 600 nm, (c) 500 nm, and (d) 400 nm.